LIMITS ON LINE BISECTOR VARIABILITY FOR STARS WITH EXTRASOLAR PLANETS

M. S. Povich,[1] M. S. Giampapa,[2] J. A. Valenti,[3,4] T. Tilleman,[2] S. Barden,[3] D. Deming,[5] W. C. Livingston,[2] AND C. Pilachowski[3]

ABSTRACT

We present an analysis of high-resolution synoptic spectra of ten F- and G-type stars, seven of which exhibit periodic radial velocity variations due to the presence of one or more substellar companions. We searched for subtle periodic variations in photospheric line asymmetry, as characterized by line bisectors. In principle, periodic variations in line asymmetry observed at lower spectral resolution could mimic the radial velocity signature of a companion, but we find no significant evidence of such behavior in our data. Observations were obtained from 1998 March to 1999 February using the National Solar Observatory (NSO) 1.52 m McMath-Pierce Solar Telescope Facility on Kitt Peak in conjunction with the solar-stellar spectrograph, achieving a resolving power of 1.2×10^5. To characterize line asymmetry, we first measured line bisectors for the unblended Fe I photospheric line at 625.26 nm. To improve sensitivity to small fluctuations, we then combined points in each bisector to form a velocity displacement with respect to the line core. We searched for periodic variations in this displacement, finding no substantial difference between stars with substellar companions and those without reported companions. We find no correlation between bisector velocity displacement and the known orbital phase of substellar companions around our target stars. Simulations of a periodic signal with noise levels that mimic our measurement errors suggest that we can exclude bisector variations with amplitudes greater than about 20 m s^{-1}. These results support the conclusion that extrasolar planets best explain the observed periodic variations in radial velocity.

Key words: line: profiles — planetary systems — stars: late-type

1. INTRODUCTION

High-precision radial velocity studies of nearby stars have resulted in the first detections of extrasolar planetary systems, consisting primarily of "massive Jupiters" (Mayor & Queloz 1995; Marcy & Butler 1998, and references therein). These detections rely on achieving precisions of 3–15 m s^{-1}. Stellar activity in the form of spots and plages, nonradial pulsations, and convective inhomogeneities combined with rotation can distort stellar photospheric lines beyond the intrinsic asymmetries arising from surface convection, thereby contributing error in the form of "stellar noise" to sensitive radial velocity measurements (Saar & Donahue 1997; Hatzes 1996). Further improvement in radial velocity precision beyond this intrinsic variability limit will require increased attention to line-profile perturbations caused by stellar atmospheric phenomena. In particular, changes in line shape arising from stellar atmospheric motion can mimic small radial velocity variations at the spectral resolution ($R \sim 5-7 \times 10^4$) typically utilized for planet searches.

Convection in the photosphere consists of rising, hotter material (associated with bright granules on the Sun) and falling, cooler material (e.g., the intergranular lanes), yielding a superposition of two profiles shifted relative to each other. The net profile is asymmetric because of unequal contributions from the rising and falling components. In the Sun, the asymmetry appears as a C-shaped curvature of the line bisector, which is the locus of points midway between the red and blue wings of a spectral line. The bisector is defined and discussed extensively by Gray (1988 and references therein), especially within the context of convection in late-type stars.

Gray (1997) originally suggested that subtle temporal variations in ($R \sim 10^5$) line bisectors for 51 Peg might be the source of radial velocity variations attributed to the gravitational influence of a planetary companion. Gray's (1997) challenge of the planetary companion hypothesis was based on a sparse data-set that appeared to show regular variations in the bisector span of an Fe I photospheric line with a period equal to the orbital period of the putative planet. However, subsequent investigations by Gray (1998) and Hatzes, Cochran, & Bakker (1998) based on an intensive series of observations of 51 Peg did not detect any systematic changes in the line shapes that could be misinterpreted as radial velocity shifts. Thus, the data are most compatible with the presence of a sub-stellar mass companion to 51 Peg.

Following the challenge by Gray (1997), we initiated a long-term program of high spectral resolution observations of seven late-type stars with reported planetary companions along with three additional late-type stars with no known substellar companions down to the sensitivity limits of current radial velocity monitoring programs. We note that François et al. (1999) also conducted an intensive series of high spectral resolution observations of 51 Peg and υ And over four nights at the Canada-France-Hawaii Telescope (CFHT). These investigators did not observe any regular change in line bisector shape that could give rise to spurious

---

[1] National Solar Observatory, Research Experiences for Undergraduates, summer 1999. Also at Department of Astronomy, Harvard University, Cambridge, MA 02138.

[2] National Solar Observatory, National Optical Astronomy Observatory, P.O. Box 26732, Tucson, AZ 85726-6732. The National Solar Observatory and the National Optical Astronomy Observatory are each operated for the National Science Foundation by the Association of Universities for Research in Astronomy, Inc.

[3] National Optical Astronomy Observatory, Tucson, AZ 85726-6732.

[4] Now at Space Telescope Science Institute, 3700 San Martin Drive, Baltimore, MD 21218.

[5] NASA/Goddard Space Flight Center, Code 693, Greenbelt, MD 20771.

Doppler shifts occurring with the period of the planetary companion. Our investigation extends these studies through the addition of a longer temporal baseline of relatively frequent observations of several late-type stars reported to have planetary companions.

2. OBSERVATIONS AND REDUCTION

The spectra were obtained with the 1.52 m main telescope of the NSO/Kitt Peak McMath-Pierce Solar Telescope Facility in conjunction with the stellar spectrograph. The stellar spectrograph is described by Smith & Giampapa (1987). We utilized the echelle grating with the 180 mm Nikon transfer lens, TI 800×800 UV-enhanced CCD and a 10×200 mm Bowen-Walraven image slicer. This configuration yielded a resolution of $R = 1.20 \times 10^5$ as measured directly from the full widths at half-maximum (FWHMs) of the ThAr comparison source lines. All spectra were centered on the Fe I photospheric absorption line at 625.3 nm used by Gray (1998) in his study of 51 Peg. The program stars are presented in Table 1.

A quartz lamp and a ThAr comparison source were utilized for flat fielding and wavelength calibration, respectively. A barycentric correction was applied so that all spectra for a given program star are on a uniform wavelength scale. While not essential for the analysis of profile shapes, this facilitated the combining of multiple frames, including the construction of a very high signal-to-noise ratio average spectrum that is used as a template spectrum for the error analysis (§ 2.2).

Our initial inspection of the reduced spectra revealed line depth variations in photospheric features on a night-to-night basis. This *apparent* variability of the line strength is an artifact which likely is related to the uneven illumination of the slicer assembly by the stellar image in conditions of variable seeing. Extraction of the individual slicer spectra showed that the more faintly illuminated slices yielded shallower absorption features. To each spectrum, we added an empirical " background " correction, x, and then renormalized the continuum, obtaining

$$S_{\text{corr}} = \frac{S + x}{1 + x}, \qquad (1)$$

where S is the original reduced spectrum and S_{corr} is the corrected spectrum. This approach yielded individual slicer spectra with equal line depths. For 55 Cnc, the background correction required to match all the slices also yielded line depths in agreement with a spectrum obtained independently by G. Marcy using the Lick Hamilton echelle. The excellent agreement between the spectra validated our empirical correction scheme.

We constructed a reference spectrum for each star by reducing and summing spectra from three separate images (see Fig. 1). The remaining spectra for that star were then mapped to the reference spectrum, using a nonlinear least-squares fitting routine that quadratically mapped each individual wavelength scale onto the reference wavelength scale, fit a polynomial to match the continua, and applied a background correction of the form in equation (1) to yield a set of consistent spectra. Finally, we created a high signal-to-noise ratio (S/N > 1500) template spectrum for each of our target stars by combining all the individual dithered spectra using an Interactive Data Language (IDL) routine which performs neighborhood averaging on unevenly sampled data. This template spectrum is used to estimate bisector errors (§ 2.2).

2.1. *Line Bisector Analysis*

We construct the bisector for the Fe I 6252.6 Å line following the method described by Gray (1988). Specifically, we locate the pixel closest to the line core and then step up the blue side of the profile pixel by pixel. From each blue pixel, we extend a horizontal (i.e., same level of residual intensity) line segment across the profile. The wavelength value for the red end of the segment is determined though linear interpolation between the neighboring pixels. The bisector connects the midpoints of these line segments. We adopt linear interpolation because error propagation is more straightforward, bisector points are more independent of one another, and outliers do not cause ringing. There is likely some curvature across a pixel, especially in the line core, but we fitted the line core with a parabola and curvature is minimal in the steep part of the line profiles, where we use linear interpolation. In addition, the points on one side of the profile are used without interpolation which further mitigates the effect of curvature. Typically, we used seven bisector points for Fe I 6252.6 Å in G-type stars and twelve bisector points for the more rotationally broadened F-type stars. A typical line bisector is illustrated in Figure 2.

TABLE 1
TARGET STARS

HR	Name	Type	Period[a] (days)	T_0[a,b]	K (m s^{-1})
458	v And[c]	F8 V	4.6163	50542.736	60.1
1101	10 Tau	F9 IV–V	...	...	...
3522	55 Cnc	G8 V	14.6597	50484.188	72.8
4277	47 UMa	G1 V	1026.58	50405.303	47.1
5072	70 Vir	G4 V	116.666	50539.287	317.0
5185	τ Boo	F6 IV	3.31253	50537.569	468.2
5933	γ Ser	F6 IV–V	...	...	...
5968	ρ CrB	G0 Va	39.8412	50975.357	60.7
7503	16 Cyg A	G1.5 Vb	...	...	...
8729	51 Peg	G2.5 IVa	4.23110	50509.695	56.1

[a] Calculated from data courtesy G. Marcy.
[b] JD $-2,400,000$.
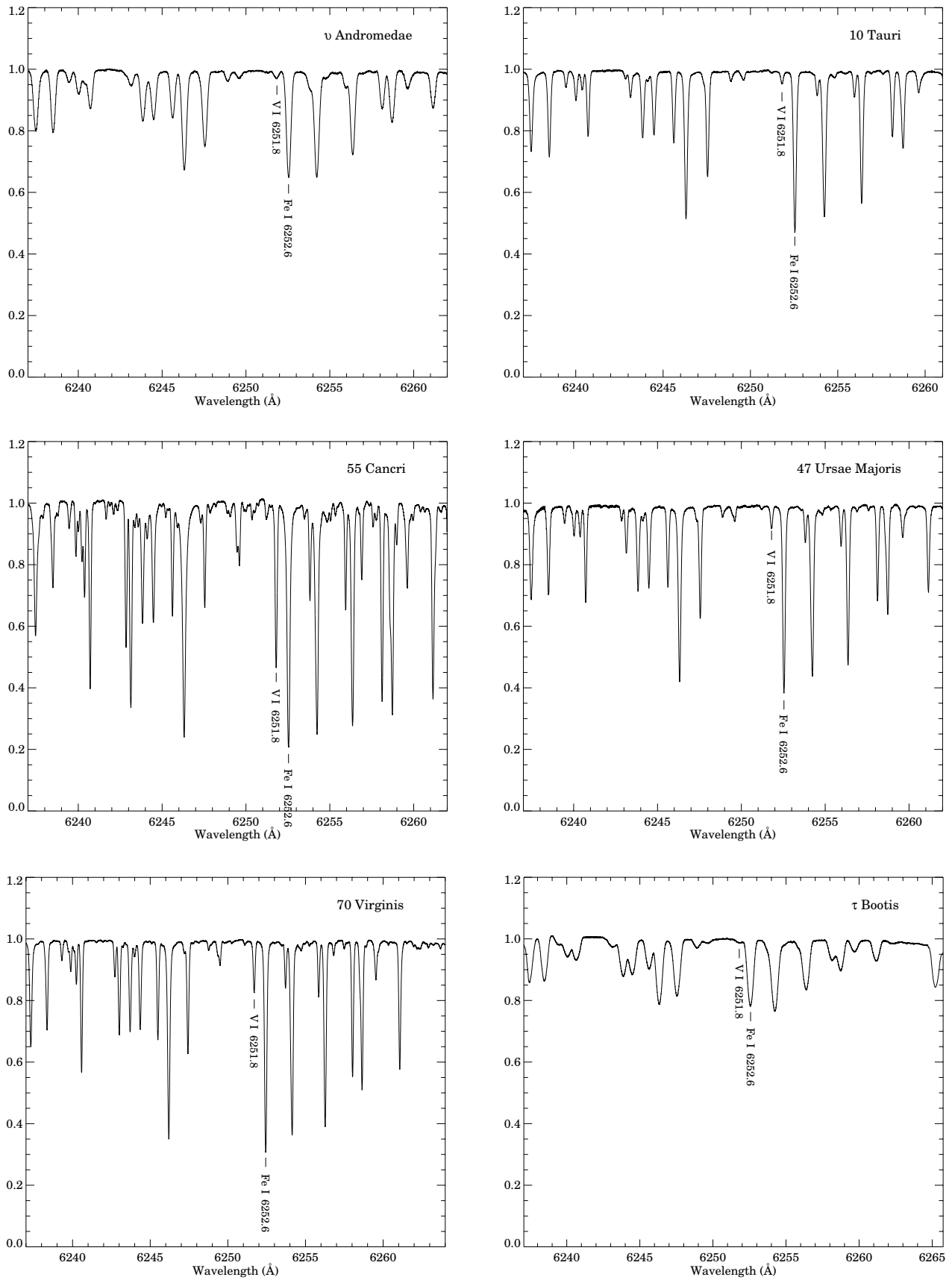[c] Multiple planet system–Doppler parameters are given for the innermost companion only (v And b).

Fig. 1.—Template spectra of all the stars in our data set. Spectral resolution ($\lambda/\delta\lambda$) is $\simeq 1.2 \times 10^5$ with S/N > 1500. The F-type stars (see Table 1) exhibit shallower, rotationally broadened absorption lines. The spectrum of 55 Cnc contains many more lines than are seen in our other target stars, most likely due to an enhanced CN content in the photosphere.
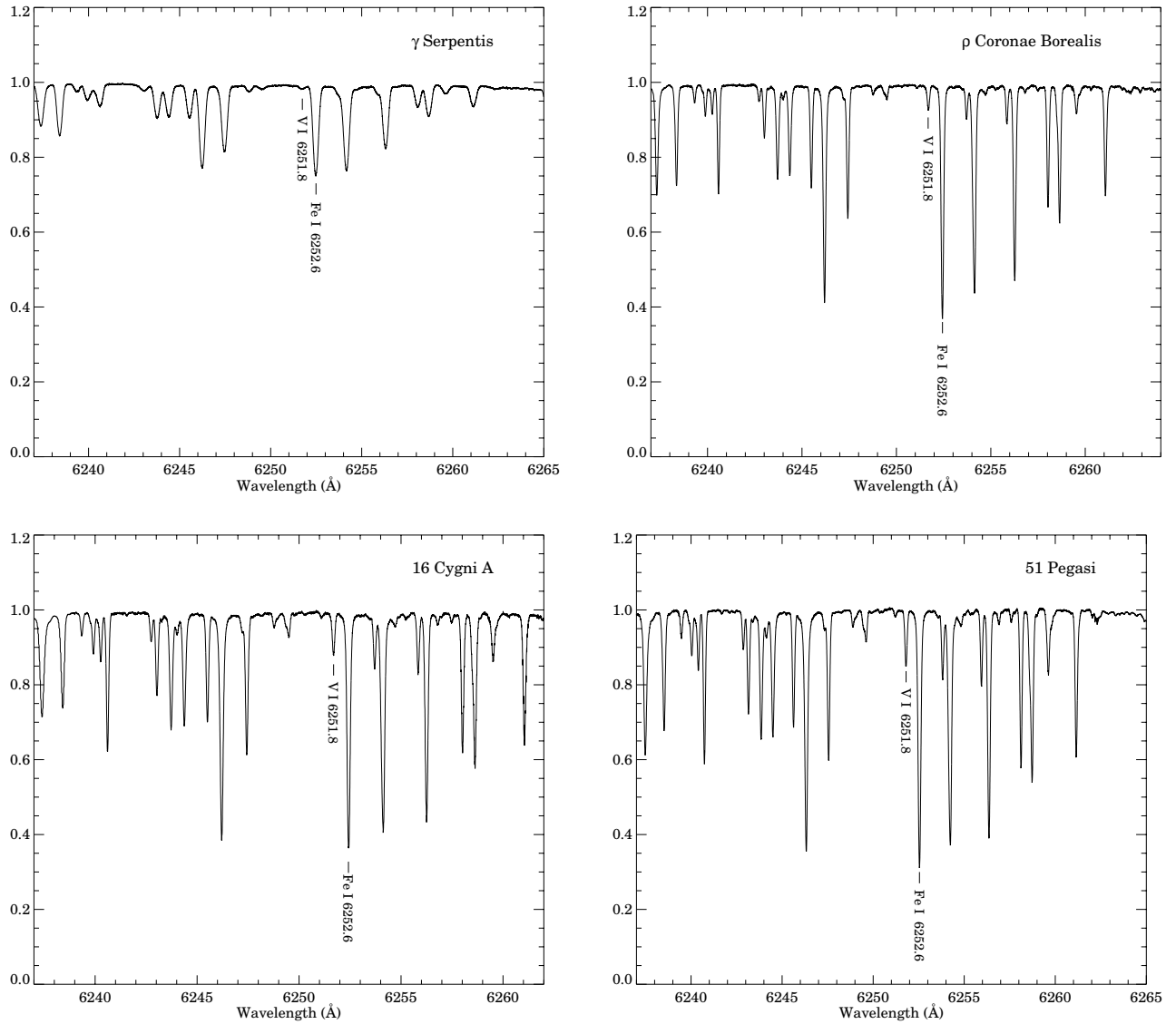
FIG. 1.—*Continued*

Once we have derived the bisector, we measure velocity offsets v_1, v_2, and v_3, corresponding to residual intensities y_1, y_2, and y_3 (see Fig. 2). Velocity offsets are measured with respect to the center of a parabolic fit to the line core. We determine v_i for a given y_i by linear interpolation of adjacent bisector points. Following Gray (1998) and Gray & Hatzes (1997), we chose $(y_1, y_2, y_3) = (0.83, 0.7, 0.5)$ for the Fe I line, which for 51 Peg has a residual intensity of $\simeq 0.3$ in the core. For other stars, the measurement depths, y, were scaled according to observed line depth.

Line asymmetries are typically characterized by velocity span (or amplitude) or bisector curvature. For example, the former approach is used by Livingston et al. (1999) to measure line-profile asymmetry in solar spectra. Livingston et al. (1999) define the bisector amplitude as $a_b = \lambda_c - x_{min}$, where λ_c is the observed central wavelength of the absorption feature and x_{min} is the most extreme blue point in the bisector. This approach is especially appropriate for solar observations where the combination of very high spectral resolutions ($R \gtrsim 3 \times 10^5$) and S/N ($\gtrsim 5000$) yields well-defined bisectors with a large number of independent points. Consequently, derivatives of the bisector itself can be determined and x_{min} can be deduced through mini-

mization. This method is usually not feasible for stellar observations which are typically characterized by lower spectral resolution and S/N. In the context of this investigation, we define the velocity span as

$$v_s = v_3 - v_1 . \qquad (2)$$

The other principal measure of line asymmetry is bisector curvature, which has been described as the difference between bisector spans computed for the top and bottom halves of a line (Gray & Hatzes 1997; Gray 1998). In our terminology, this is equivalent to

$$c_b = (v_3 - v_2) - (v_2 - v_1) . \qquad (3)$$

Since the curvature, c_b, is a second derivative (whereas span is a first derivative), the signal-to-noise requirements are more demanding in order to obtain significant measures of variability in the bisector curvature. We therefore adopted an alternative characterization which is a variant of the span method designed to increase sensitivity. We define this velocity displacement as

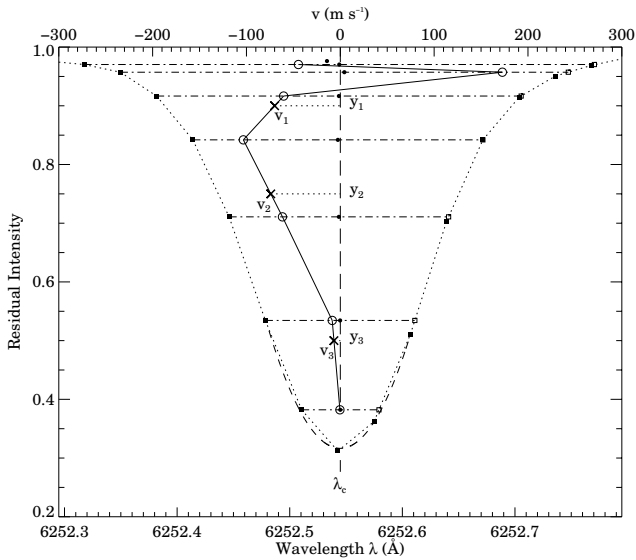$$v_b = \frac{v_1 + v_2 + v_3}{3} - \lambda_c , \qquad (4)$$

FIG. 2.—Schematic diagram of a spectral line bisector, illustrating the C shape and evaluation points v_1, v_2, and v_3 (*plotted as times cross*). The bisector points (*small filled circles*) are the midpoints of the horizontal, dashed-dotted line segments, plotted on the wavelength scale of the spectrum. Filled squares are data points in the observed spectrum, while open squares indicate where linear interpolation has been used to determine the red endpoints of the bisector segments. The solid line with large, open circles is the entire bisector, plotted on the velocity (v) scale, which is expanded by a factor of 40 relative to the wavelength scale. Zero velocity is defined as λ_c, determined from a parabola fit to the line core (*dashed curve*).

where v_b is the average displacement of the evaluation points from the line core.

A comparison of the formulations in equations (2)–(4) suggests that for a C-shaped bisector, v_b and v_s will be negative while the curvature, c_b, will be positive. The principal advantage of v_b as defined by equation (4) is that by utilizing the average of all three evaluation points, the impact of the uncertainties in individual evaluation points is mitigated. We also note that our method of bisector measurement relies on an accurate determination of the location of the line core (λ_c), which we ascertain by fitting a parabola to the line core.

In equation (4), averaging v_1, v_2, and v_3 reduces uncertainties relative to the separate use of these points in a first or second derivative. Uncertainties in the velocity shift of the line core are reduced by fitting a parabola to a few points in the line core. In essence, we are utilizing two averaged points for the determination of the bisector amplitude. In contrast, the curvature formulation in equation (3) uses three independent points with one point (v_2) used twice. We find from our data that this latter approach significantly increases measurement uncertainties (see § 2.2).

Finally, we do not include any additional bisector points in the construction of v_b since shallower points are intrinsically noisy and only further increase the uncertainty in v_b. Deeper points impinge on the line core, which would compromise the independence of our two bisector span reference points.

2.2. *Error Analysis*

To estimate noise in the continuum, we divide each spectrum by a summed template spectrum, which is essentially noiseless. We then calculate the standard deviation of this ratio in continuum windows where the residual intensity of

the template is between 0.95 and 1.02. We assign uncertainties (σ_s) to every point in the spectrum by multiplying the continuum uncertainty by the square root of the residual intensity. In other words, we assume that uncertainties are controlled by Poisson statistics in the stellar signal, which is approximately true for these bright stars.

Uncertainties in residual intensity first propagate into our bisector determination when interpolating the red wing of the profile as illustrated in Figure 2. Uncertainty in the wavelength corresponding to a particular residual intensity is given by

$$\sigma_w = \sigma_s/m ,\qquad(5)$$

where m is the slope of the spectrum (Gray 1988), which is measured using the essentially noiseless template. We then propagate errors through successive steps in the bisector construction and interpolation onto reference depths (y) to obtain σ_1, σ_2, and σ_3, which are the uncertainties in v_1, v_2, and v_3, respectively. Uncertainty in the wavelength of the line core, σ_{λ_c}, is derived from estimated uncertainties in the residual intensity points being fitted. The final error in v_b is

$$\sigma_b^2 = \frac{\sigma_1^2 + \sigma_2^2 + \sigma_3^2}{9} + \sigma_{\lambda_c}^2 .\qquad(6)$$

The observed scatter in bisector velocity displacement is consistent with the formal uncertainties calculated in this manner, as discussed below.

We also examined the uncertainties associated with other methods of characterizing bisectors, namely span and curvature. In particular, the uncertainty in span from equation (2) is

$$\sigma_s^2 = \sigma_1^2 + \sigma_3^2 ,\qquad(7)$$

while the uncertainty in curvature from equation (3) is

$$\sigma_c^2 = \sigma_1^2 + 4\sigma_2^2 + \sigma_3^2 .\qquad(8)$$

In Table 2, we compare various characterizations of line bisectors for 51 Peg, namely, velocity displacement (v_b), span (v_s), and curvature (c_b). For each technique, we give the weighted mean of all measured values for 51 Peg (col. [2]), the standard deviation about the mean (col. [3]), and the average formal uncertainty (col. [4]). The last column contains the observed standard deviation divided by the average formal error. Values near unity indicate that our estimates of formal uncertainty provide a realistic indicator of actual errors.

Table 2 shows that for our data, velocity displacement as defined in equation (4) yields smaller formal errors than span or curvature. Moreover, the mean velocity displacement is as large as other characterizations, making v_b the most sensitive diagnostic of variability. Since our purpose here is to search for periodicity in bisector behavior, we

TABLE 2
BISECTOR AMPLITUDES FOR 51 PEG

Measure[a] (1)	Mean (m s^{-1}) (2)	Scatter (m s^{-1}) (3)	Error (m s^{-1}) (4)	Ratio
v_b	−15	42	29	1.45
v_s	2	83	61	1.36
c_b	14	53	88	0.60

[a] Bisector amplitudes: v_b is defined by eq. (4); v_s is given by eq. (2); c_b is calculated according to eq. (3).

TABLE 3

SUMMARY OF RESULTS

HR (1)	Name (2)	Type (3)	$\langle v_b \rangle$ (m s^{-1}) (4)	$\langle \sigma \rangle$ (m s^{-1}) (5)	σ_μ (m s^{-1}) (6)	N_{obs} (7)
458	υ And	F8 V	12	81	16	64
1101	10 Tau	F9 IV–V	31	36	6	80
3522	55 Cnc	G8 V	−41	36	4	225
4277	47 UMa	G1 V	−3	43	6	121
5072	70 Vir	G4 V	−17	32	4	135
5185	τ Boo	F6 IV	−45	200	22	118
5933	γ Ser	F6 IV–V	46	129	15	120
5968	ρ CrB	G0 Va	5	33	4	105
7503	16 Cyg A	G1.5 Vb	−15	42	5	82
8729	51 Peg	G2.5 IVa	−15	29	4	115

adopt the formulation that provides the strongest constraints on bisector amplitude variations, namely velocity displacement. For illustrative purposes only, we present in Figure 3 bisector curvature and span versus orbital phase for 51 Peg.

3. RESULTS AND DISCUSSION

3.1. *Significance of Variability*

In Table 3 we summarize our measurements and formal errors. Column (4) gives the mean of v_b for individual observations, weighted by their corresponding uncertainties. Column (6) gives the formal uncertainty in the weighted mean, σ_μ, calculated from uncertainties in v_b for each observation. See equation (4.31) of Bevington & Robinson (1992) for details. Column (5) gives the mean value of the formal errors, $\langle \sigma \rangle$. Measurements for each night are depicted graphically as time series in Figure 4. For convenient reference, $\langle v_b \rangle$, σ_v, and $\langle \sigma \rangle$ are given in the figure.

A key goal of this investigation is to test whether line asymmetries vary periodically on time scales consistent with precisely measured radial velocity variations. For each star, we plot in Figure 5 bisector velocities as a function of Julian date and orbital phase, as computed from planetary orbital periods and reference times (T_0) in Table 1. At the reference time, the radial velocity transitions from negative

to positive. Inspection of Figure 5 reveals no obvious periodic variability in bisector velocity displacement, though excursions for individual observations may be marginally significant in some cases.

In Table 4 we present the ratio of the observed scatter, σ_v, to the mean of the formal errors, $\langle \sigma \rangle$. This quantity is analogous to the last entry in the first row of Table 1, but for all stars. For ratios greater than unity, bisector variations may be significant, even if not periodic. A comparison of the mean value of this ratio for stars with planets com-

TABLE 4

RATIOS OF SCATTER TO MEAN UNCERTAINTIES

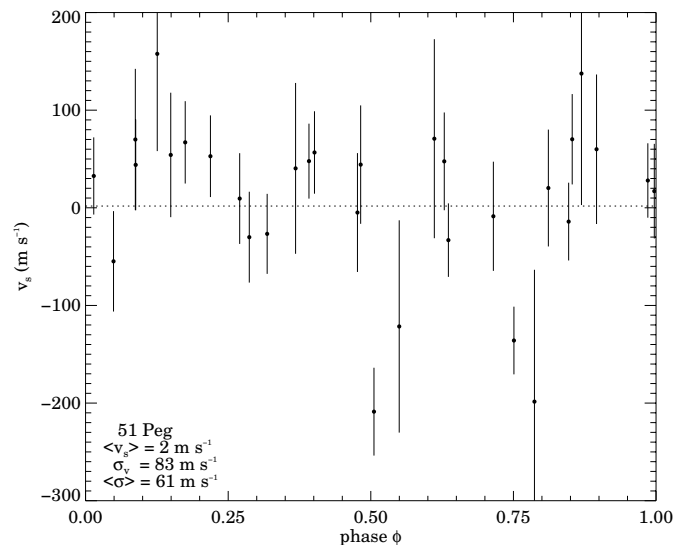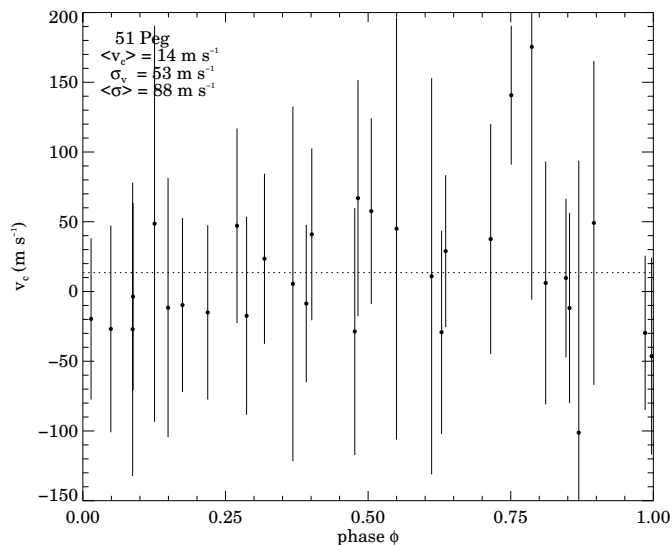| HR	Name	Type	$\sigma_v/\langle \sigma \rangle$
458	υ And	F8 V	0.7
1101	10 Tau	F9 IV–V	1.1
3522	55 Cnc	G8 V	1.5
4277	47 UMa	G1 V	1.1
5072	70 Vir	G4 V	1.2
5185	τ Boo	F6 IV	0.7
5933	γ Ser	F6 IV–V	0.6
5968	ρ CrB	G0 Va	1.4
7503	16 Cyg A	G1.5 Vb	0.9
8729	51 Peg	G2.5 IVa	1.4

FIG. 3.—Time series of bisector amplitudes for 51 Peg according to (*a*) the curvature method and (*b*) the span definition
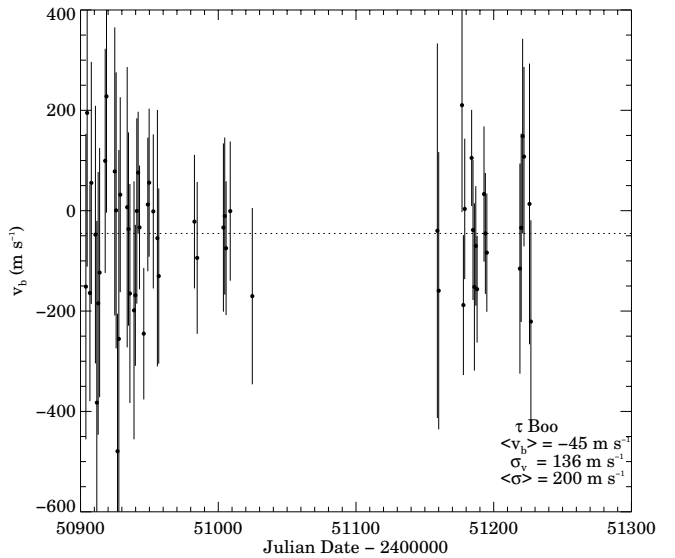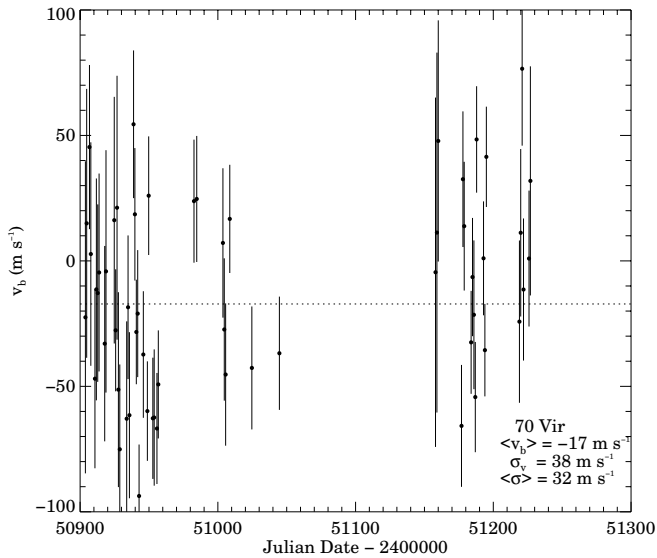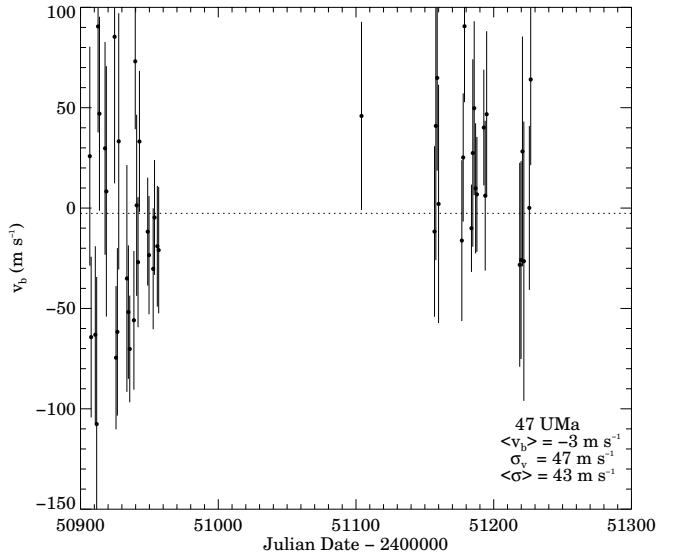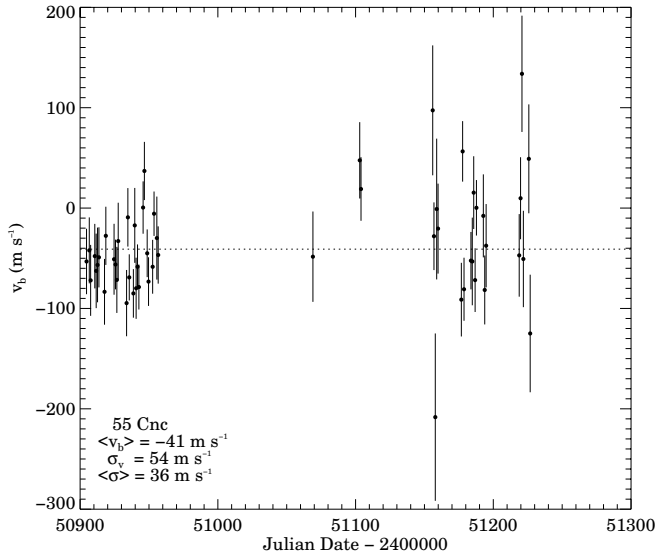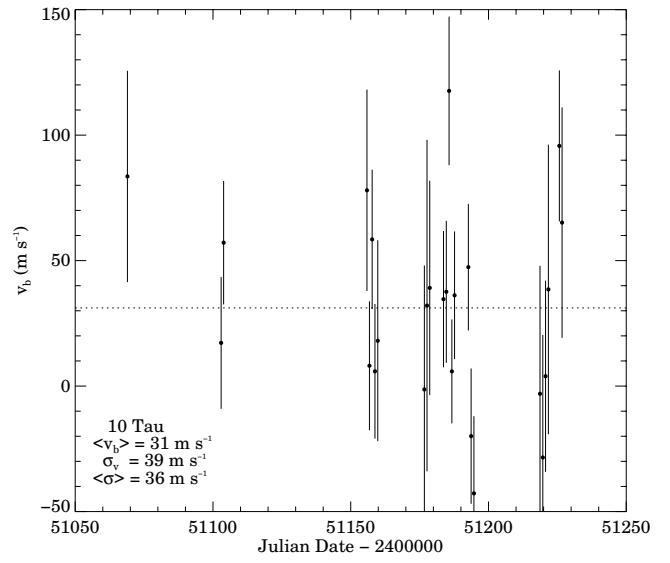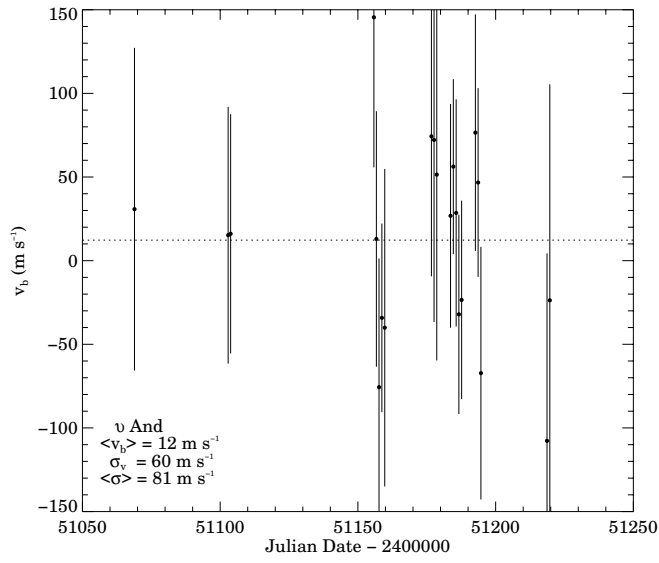
Fig. 4.—Time series of bisector amplitudes for the program stars. The dotted line on each plot denotes $\langle v_b \rangle$, the weighted mean value of v_b calculated using the formal errors. Also given are σ_v, the variance of the distribution of v_b and $\langle \sigma \rangle$, the mean value of the formal errors.
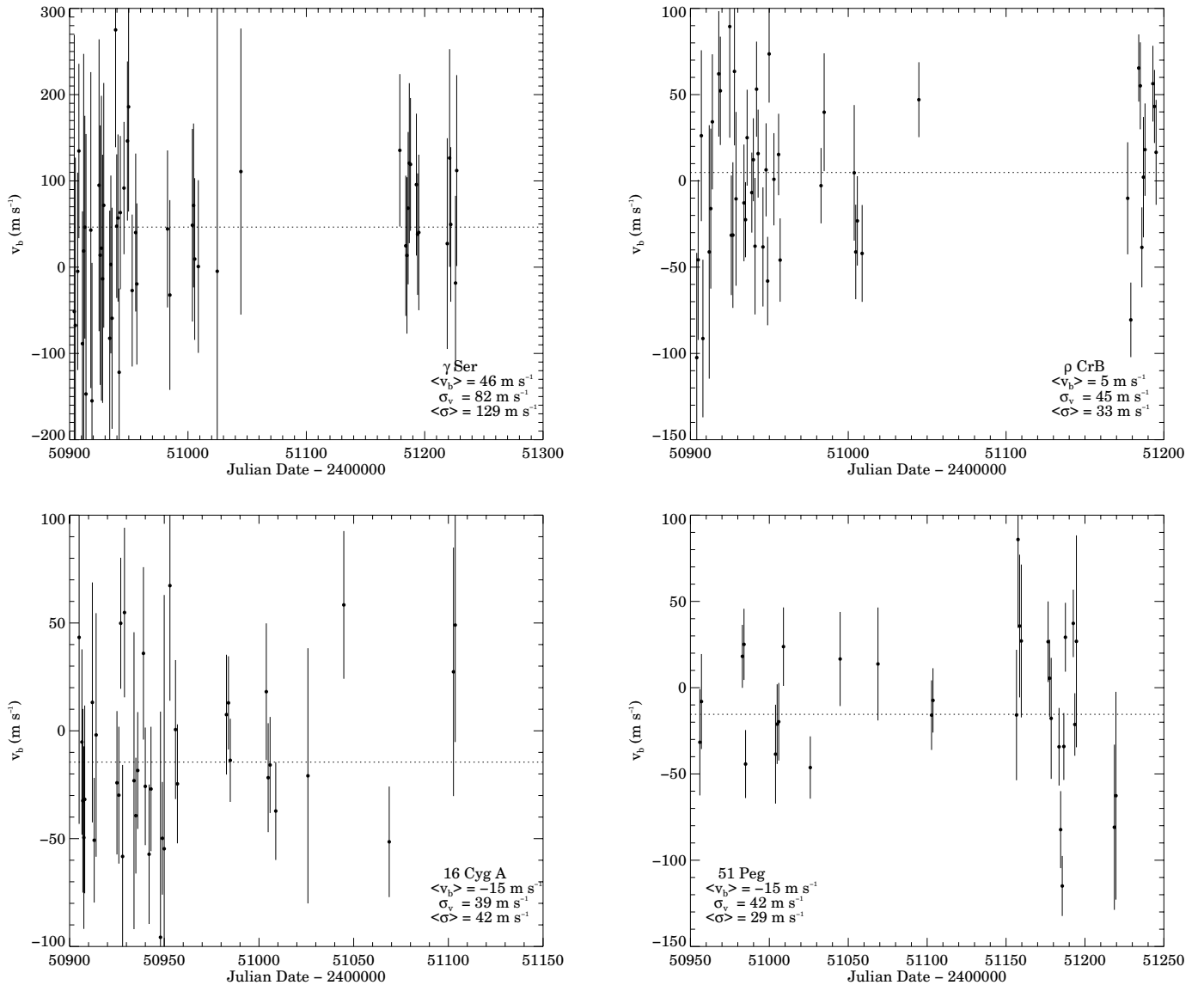
FIG. 4.—*Continued*

pared to those without planets (10 Tau, γ Ser, and 16 Cyg A) yields values of 1.1 and 0.9, respectively. We conclude that there is no significant statistical difference in the behavior of line asymmetry in stars with and without detected planets.

3.2. *Periodogram Analysis*

An important question is whether periodic variations in bisector amplitude translate into periodic, *apparent* Doppler shifts in line profiles observed at moderate resolution, thus mimicking the radial velocity signature of a very low mass (planetary) companion. While it is plausible that variations in line asymmetry may lead to subtle, apparent Doppler shifts, quantifying this assertion is difficult. In the absence of suitable hydrodynamic calculations or even empirical data relating changes in line bisector amplitude to apparent Doppler shifts, we can only crudely estimate the magnitude of the effect. Certainly, we can expect that any apparent change in stellar radial velocity, Δv_r, would be such that $\Delta v_r \lesssim \Delta v_b$. Inspection of Figure 1 suggests that $\Delta v_r \lesssim \Delta v_b/2$ is a more realistic estimate of the magnitude of the change. Thus, changes in bisector amplitude of at least 100 m s^{-1} would be required to create intrinsic variations

comparable to the 56 m s^{-1} radial velocity variations seen in 51 Peg.

We performed a periodogram analysis of the v_b time series for each star (Fig. 4), using an algorithm from Press & Rybicki (1989). Upon computing false alarm probability levels and examining the periodograms, we did not find any significant peaks at the planetary orbital period or any other period. This test is less sensitive than specifically searching for periodic variability at the period determined by precision radial velocity studies, but provides new constraints on the existence of periodic variations on other time scales.

3.3. *Sensitivity Estimates*

We also ran simulations incorporating our measurement uncertainties and actual observing windows to determine our sensitivity to signals varying at the planetary orbital period. The results indicate that except for υ And, we could have detected the presence of a continuous periodic signal at the planetary orbital period with an amplitude equal to the measured amplitude of radial velocity variations. For υ And, errors in measured bisector amplitude are too large to
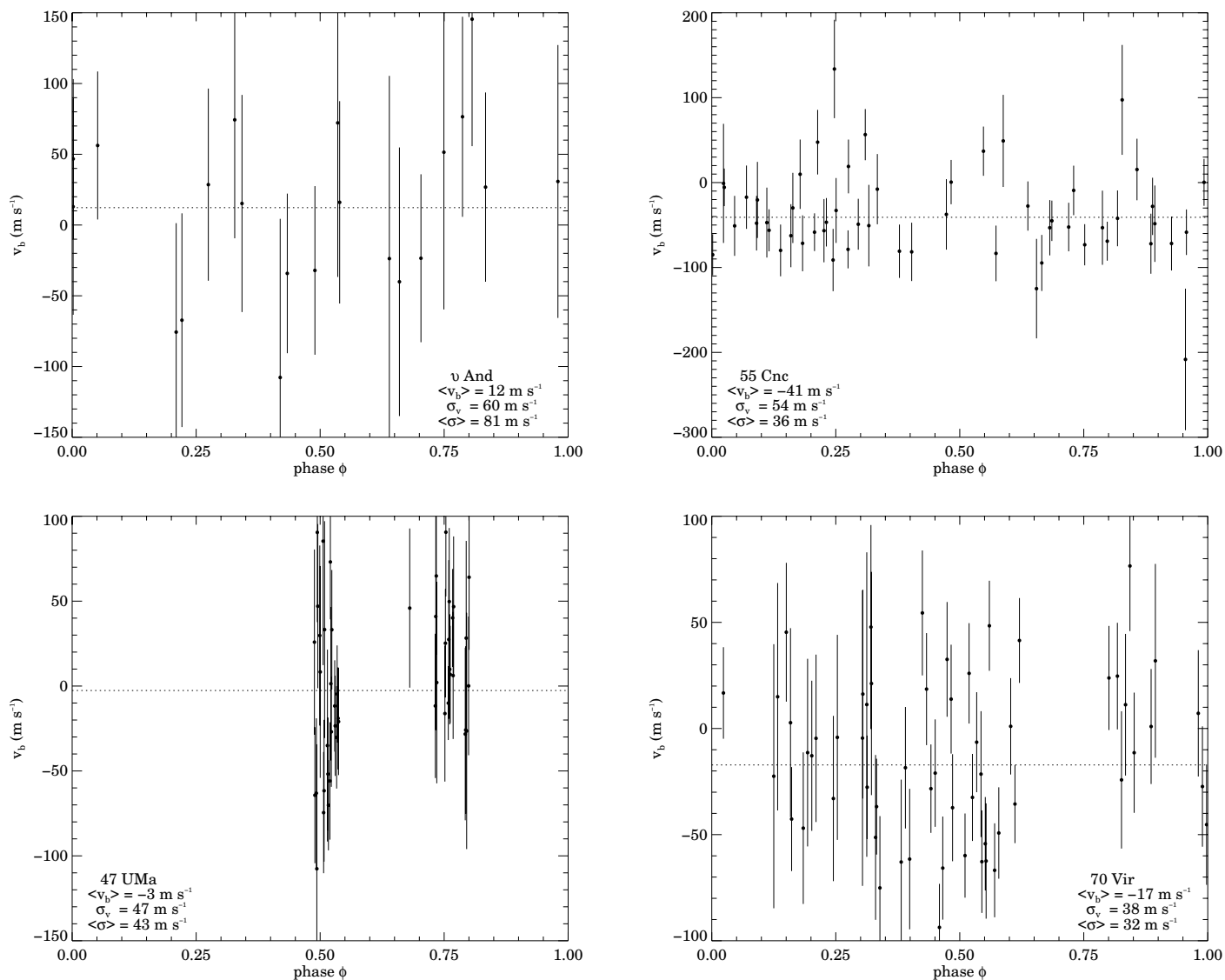
Fig. 5.—Plots of v_b vs. phase ϕ for those stars exhibiting periodic Doppler velocity variations due to the presence of a substellar companion. Orbital phase of the companion was computed from the parameters listed in Table 1.

permit detection of a periodic signal with this amplitude. The high $v \sin i$ and the relatively low amplitude of radial velocity variation, along with our errors, would mask any regular variations in v_b that might be present. In all other program stars with planets, the periodogram readily revealed the simulated periodic signal with false alarm probabilities that ranged from about several times 10^{-2} to $\sim 10^{-11}$. We conclude that for these stars, changes in line asymmetry are not the major cause of observed radial velocity variations.

For illustrative purposes, we present in Figure 6 the periodogram for the 51 Peg time series of observations along with a simulation that includes a periodic signal at the orbital period and the velocity amplitude of the reported planet. In the specific case of 51 Peg, we performed simulations for a range of amplitudes extending from 5 m s^{-1} to 50 m s^{-1}. The results reveal that variations at the orbital period with an amplitude of only 25 m s^{-1} are readily detectable within our errors at a false alarm probability $\sim 10^{-3}$. But at amplitudes as small as 10 m s^{-1}, any such regular variations that may be present would not be discernible in our data.

3.4. Trend with Spectral Type

Finally, we display in Figure 7 mean bisector velocity displacement $\langle v_b \rangle$ as a function of $B-V$ color. Inspection of Figure 7 suggests that the $\langle v_b \rangle$ is correlated with stellar spectral type, a result that is consistent with Gray (1988). In particular, Gray (1988) notes that the redward turn of the bisector in the line core (the bottom part of the C) is absent in early-type stars, only manifesting itself near spectral type G0. We would expect stars showing only the top of the C to have positive v_b, and this is indeed what we observe for most of our F stars. For cooler stars, the velocity displacement becomes more negative. Note that 55 Cnc (G8V) is the only star in our sample with molecular CN lines visible in our summed templates. The blue wing of the Fe I 6252.6 Å line is blended with a line of CN, which may affect our bisector characterization for 55 Cnc.

The significant departure of τ Boo from the trend shown in Figure 7 may be related to its relatively rapid rotation period of 3.3 ± 0.5 days (Baliunas et al. 1997). As discussed by Gray (1988), and confirmed in the case of the Sun by Smith, Huang, & Livingston (1987), line asymmetries as
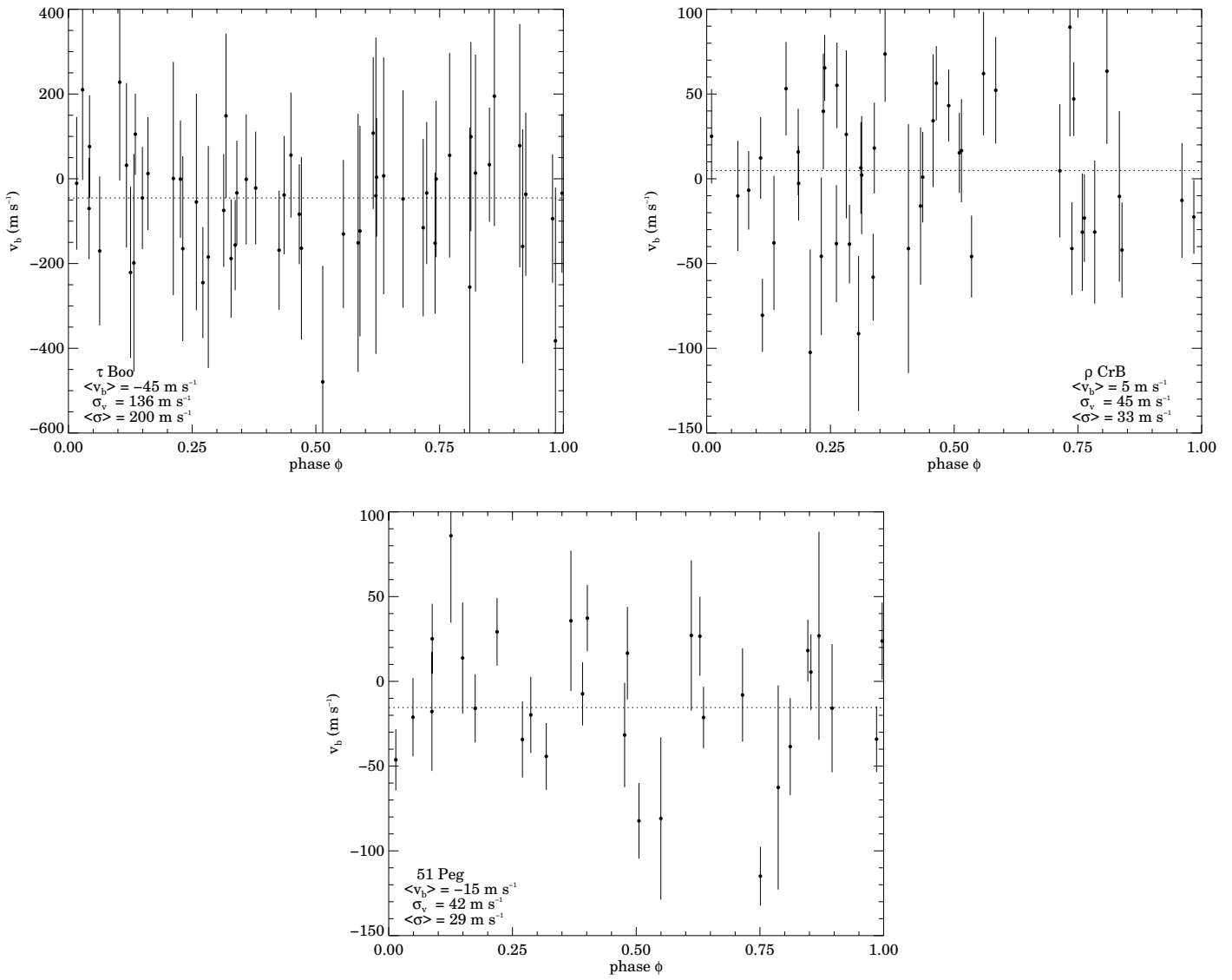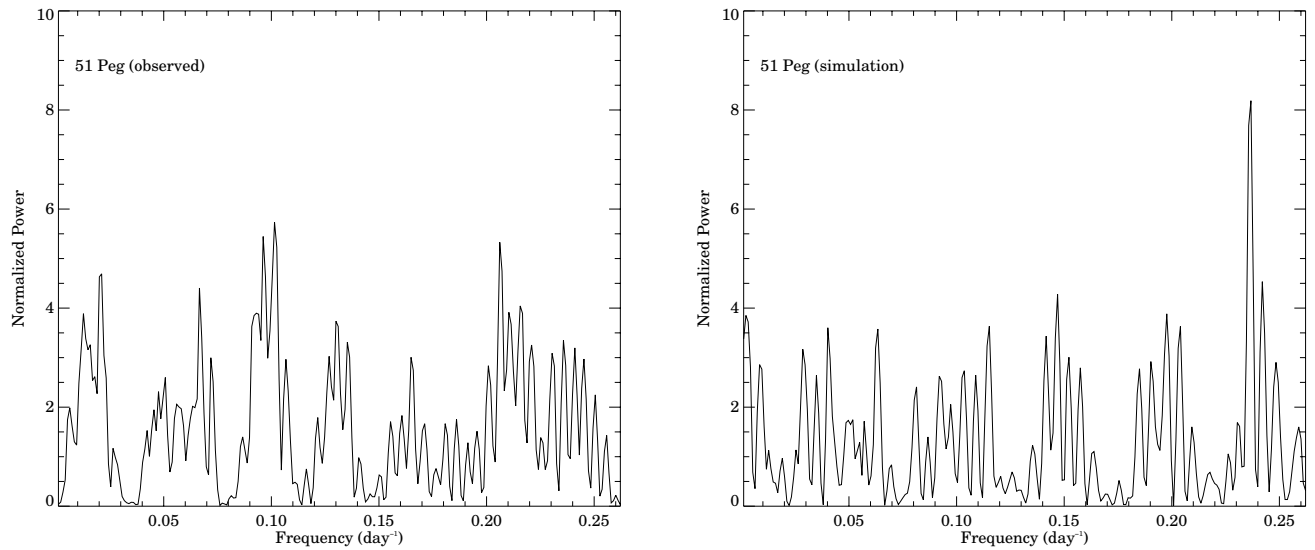
FIG. 5.—*Continued*

FIG. 6.—Periodograms computed for the observed time series for 51 Peg (*left*) and a simulation assuming a periodic signal at the planetary orbital period (*right*). The simulation incorporates the observing window and errors that are present in the left panel. No significant peaks are seen in the observational data. A significant feature is evident in the simulation at a frequency of 0.2373 day^{-1}, corresponding to a period of 4.214 days, near the planetary orbital period of 4.231 days.
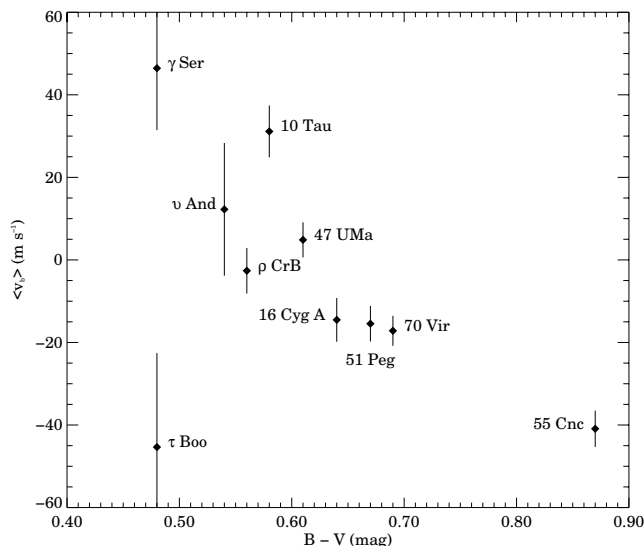
FIG. 7.—Mean bisector velocity displacement plotted against spectral type of each star. The transition from negative to positive values of $\langle v_b \rangle$ toward earlier-type stars could be interpreted as movement up the **C** (see text).

characterized by the amplitudes of line bisectors can be enhanced by rotational redistribution of the Doppler shifts arising from the granular motions. In essence, rotation adds a velocity component to the line-of-sight motion of granules with the effect most pronounced at the equatorial limbs. Certainly, the results in Figure 7 for τ Boo are qualitatively consistent with the nature of this so-called "rotation effect."

Alternatively, the coincidence of the stellar rotation period with the ≈ 3.3 day orbital period of the planetary companion raises the speculation that the rotational synchronization via tidal locking of the planet with the star could lead to the modification of the granulation pattern in the photosphere. Cuntz, Saar, & Musielak (2000) conclude

from theoretical and empirical considerations that extrasolar giant planet systems with small separations such as τ Boo should be characterized by both strong magnetic and tidal interactions. In fact, τ Boo exhibited the strongest magnetic interaction among the stars considered in their theoretical investigation. In view of the well-known interaction between magnetic fields and convection in the Sun and late-type stars, this speculation merits investigation.

4. CONCLUSIONS

We have utilized synoptic spectroscopic observations of stars with reported planetary companions to investigate whether line-profile variability arising from stellar atmospheric motions could mimic the observed radial velocity variations. In summary, we did not find any periodic variability in the velocity amplitude of the bisector of the photospheric Fe I line at 6252.6 Å which was the focus of our investigation. Furthermore, the variations in bisector amplitudes that were detected are consistent with uncertainties expected from the propagation of errors in the original spectra. While isolated excursions in the time series of bisector amplitudes are observed that may arise from real variability, the significance is not high enough to exclude other sources of measurement error.

The behavior of our measured mean bisector velocity displacement as a function of spectral type is consistent with previous work. While line-profile variations are certainly a source of intrinsic stellar noise in Doppler spectroscopic searches at the subkilometer per second level, our results indicate that it is the presence of substellar companions which best explains the periodic variations in radial velocity that have been reported for our program stars.

REFERENCES

Baliunas, S. L., Henry, G. W., Donahue, R. A., Fekel, F. C., & Soon, W. H. 1997, ApJ, 474, L119
Bevington, P. R., & Robinson, D. K. 1992, Data Reduction and Error Analysis for the Physical Sciences (2d ed.; New York: McGraw-Hill), 64
Cuntz, M., Saar, S. H., & Musielak, Z. E. 2000, ApJ, 533, L151
François, R., Briot, D., Spite, F., & Schneider, J. 1999, A&A, 349, 220
Gray, D. F. 1988, Lectures on Spectral-Line Analysis: F, G, and K Stars (Arva, Ontario: Publisher)
———. 1997, Nature, 385, 795
———. 1998, Nature, 391, 153
Gray, D. F., & Hatzes, A. P. 1997, ApJ, 490, 412
Hatzes, A. P. 1996, PASP, 108, 839
Hatzes, A. P., Cochran, W. D., & Bakker, E. J. 1998, Nature, 391, 154
Marcy, G. W., & Butler, R. P. 1998, ARA&A, 36, 57
Mayor, M., & Queloz, D. 1995, Nature, 378, 355
Livingston, W., Wallace, L., Huang, Y., & Moise, E. 1999, in ASP Conf. Ser. 183, High Resolution Solar Physics: Theory, Observations, and Techniques, ed. T. R. Rimmele, K. S. Balasubramaniam, & R. R. Radick (San Francisco: ASP), 494
Press, W. H., & Rybicki, G. B. 1989, ApJ, 338, 277
Saar, S. H., & Donahue, R. A. 1997, ApJ, 485, 319
Smith, M. A., & Giampapa, M. S. 1987, in Lecture Notes in Physics 291, Cool Stars, Stellar Systems, and the Sun, ed. J. Linsky & R. Stencel (New York: Springer), 477
Smith, M. A., Huang, Y.-R., & Livingston, W. 1987, PASP, 99, 297